nature portfolio

https://doi.org/10.1038/s41586-022-05228-5

Supplementary information

Free-space dissemination of time and frequency with 10^{-19} instability over 113 km

Supplementary Information for "Free-space dissemination of time and frequency with 10^{-19} instability over 113 km"

Qi Shen[1,2,3,*], Jian-Yu Guan[1,2,3,*], Ji-Gang Ren[1,2,3,*], Ting Zeng[1,2,3], Lei Hou[1,2,3], Min Li[1,2,3], Yuan Cao[1,2,3], Jin-Jian Han[1,2,3], Meng-Zhe Lian[1,2,3], Yan-Wei Chen[1,2,3], Xin-Xin Peng[1,2,3], Shao-Mao Wang[1,2,3], Dan-Yang Zhu[1,2,3], Xi-Ping Shi[8], Zheng-Guo Wang[1,2,3], Ye Li[8], Wei-Yue Liu[8], Ge-Sheng Pan[1,2,3], Yong Wang[5], Zhao-Hui Li[4], Jin-Cai Wu[3,4], Yan-Yan Zhang[6], Fa-Xi Chen[7], Chao-Yang Lu[1,2,3], Sheng-Kai Liao[1,2,3], Juan Yin[1,2,3], Jian-Jun Jia[3,4], Cheng-Zhi Peng[1,2,3], Hai-Feng Jiang[1,2,3], Qiang Zhang[1,2,3,4,7], Jian-Wei Pan[1,2,3]

[1] *Hefei National Research Center for Physical Sciences at the Microscale and School of Physical Sciences, University of Science and Technology of China, Hefei 230026, China*

[2] *Shanghai Research Center for Quantum Science and CAS Center for Excellence in Quantum Information and Quantum Physics, University of Science and Technology of China, Shanghai 201315, China*

[3] *Hefei National Laboratory, University of Science and Technology of China, Hefei 230088, China*

[4] *Key Laboratory of Space Active Opto-Electronic Technology, Shanghai Institute of Technical Physics, Chinese Academy of Sciences, Shanghai 200083, China*

[5] *Xinjiang Astronomical Observatory, Chinese Academy of Sciences, Urumqi 830011, China*

[6] *Key Laboratory of Time and Frequency Primary Standards, National Time Service Center, Chinese Academy of Sciences, Xi'an 710600, China*

[7] *Jinan Institute of Quantum Technology, Jinan, Shandong 250101, China*

[8]*Faculty of Information Science and Engineering, Ningbo University, Ningbo 315211, China*

[*]*These authors contributed equally to this work.*

1 The link loss determination

In this experiment, the ratio between transmitted and received OFC power is up to a few 10^9, three orders higher than the isolation between sending and receiving optical path (approximately 60 dB). Thus, the received power can not be measured simultaneously while the link works. Here, we develop an approach to acquire the received OFC power according to the peak voltage of the LOS.

The relationship between the peak voltage and received OFC power is shown in Fig. 1(a). There is good linear relation between the peak voltage and square root of the received OFC power, i.e., $V_{peak} + V_{offset} \propto \sqrt{P_s}$. Based on this relationship, we can inversely calculate the power. However, it is not straight forward, because the LOS records signals only if the peak values exceed the threshold voltages of around 30-50 mV, corresponding to the signal power of about 2-4 nW. Here, we estimate the average power according to the valid data ratio and loss distribution, when the link loss is high.

The distribution of the link loss is measured at dusk, so that we have nearly 100% valid data to fit it. As shown in Fig. 1(b), the probability of the received OFC well fits a log-normal distribution, consistents with the atmospheric model[1]. Thus, the average power can be estimated by this distribution and the valid data ratio.

To evaluate the accuracy of this approach, we calibrate it with a commercial power meter. An optical coupler is inserted at the 1545 nm LOS of terminal A to guide 5% power to the power meter, the sending OFC power is reduced to avoid stray reflection effect, and the local OFC power at the LOS is kept the same. The measurement was repeated 10 times, and each one lasts 5,000 seconds. Fig. 2 gives the link loss obtained with two methods. The peak fitting approach provides a slightly lower link loss in comparision with that given by the power meter and the difference is below 2 dB. The corresponding valid data ratio is shown here as well.

2 Link loss simulation of the horizontal free-space channel

The whole link loss measured from the output of the comb of one terminal to the input of the balanced detector of the other terminal can be expressed by Eq. 1.

$$\begin{aligned}\eta_{link} &= \eta_{los}\eta_{tele\_link} \\ &= (\eta_{los\_t}\eta_{los\_r})(\eta_{tele\_t}\eta_{geo}T_{atm}\eta_{tele\_r}\eta_{sm}\eta_{atp}) \end{aligned} \tag{1}$$

The link loss mainly contains the LOS optics loss η_{los} and the telescope link loss η_{tele_link}. The LOS optics loss, including the transmitter loss η_{los_t} and receiver loss η_{los_t}, are around 4 dB. The telescope link loss includes other parts. η_{tele_t} and η_{tele_r} are the telescope optical efficiency of the transmitter and receiver, respectively.

The geometric attenuation is expressed as

$$\eta_{geo} = (\frac{D_r}{D_r + L\theta_t})^2, \tag{2}$$

where D_r is the apertures of the receiver telescope; L is the free-space channel distance; θ_t represents the effective transmitter full-angle divergence for the free-space link.

T_{atm} is the atmospheric transmittance[2], which is reduced by the air absorption and scattering of the propagating beam, described by the expression,

$$T_{atm} = e^{-\sigma L}, \tag{3}$$

where σ is the total extinction coefficient containing the absorption and scattering coefficients of atmospheric molecules. Since the NIR band is called the 'atmospheric window', atmospheric molecular absorption is not considered in non-rainy and foggy weather. Atmospheric molecular scattering can be handled by Rayleigh scattering theory[3].

$$\sigma = \frac{3.91}{V}(\frac{\lambda}{550nm})^{-q} \tag{4}$$

V is visibility (km), λ is the optical wavelength, and q is the size distribution of the scattering particles.

$$\begin{cases} q = 0.58V^{\frac{1}{3}}, & V \leq 6km \\ q = 1.3, & 6km < V < 50km \\ q = 1.6, & V \geq 50km \end{cases} \tag{5}$$

η_{sm} represents the single-mode fiber coupling efficiency. It is related to the parameter r_0, also called Fried's parameter[4], is usually defined by the expression,

$$r_0 = [0.42sec(\zeta)k^2 \int_{h_0}^{H} C_n^2 dh]^{-3/5} \tag{6}$$

where ζ is the zenith angle, k is the wave number of beam wave, C_n^2 is the refractive-index structure parameter, and H is the altitude of the higher site, which equals $h_0 + Lcos(\zeta)$, and h_0 represents the altitude of the lower site.

The theoretical formula for calculating the free-space single-mode coupling efficiency [5] is listed as below.

$$\eta_{sm} = 8a^2 \int_0^1 \int_0^1 \exp[-(a^2 + \frac{A_R}{A_C})(x_1^2 + x_2^2) \times I_0(2\frac{A_R}{A_C}x_1 x_2)x_1 x_2 dx_1 dx_2] \tag{7}$$

where

$$a = \frac{D_r}{2}\frac{\pi W_m}{\lambda f} \tag{8}$$

$$A_R = \frac{\pi D_r^2}{4} \tag{9}$$

$$A_C = \pi \rho_c^2 \tag{10}$$

$$\rho_c^2 = (1.46 C_n^2 k^2 L)^{-3/5} \tag{11}$$

a is the ratio of the receiver radius to the radius of the backpropagated fiber mode. D_r is the receiver lens diameter. W_m is the fiber-mode field radius at the fiber end face. λ is the optical wavelength and f is the focal length of the receiver. A_R is the area of the receiver aperture, and A_C is the spatial coherence area of the incident plane wave. ρ_c is the spatial coherence distance.

η_{atp} is the decrease in efficiency arising from the pointing error of the acquisition, tracking and pointing (ATP) system, which is typically 3 dB.

For our system, the input parameters for the total link calculation are shown in Table. 1. The telecope link loss is estimated to be 70 dB, including the telescope optical efficiency of 4.8 dB, the geometric attenuation of 21.8 dB, the atmospheric attenuation of 12.5 dB, the single-mode coupling attenuation of 27.9 dB, and the ATP loss of 3 dB. Considering the LOS optics loss of 4 dB, the total link loss is 74 dB. The simulated r0, single-mode coupling efficiency, and total link loss are shown in Fig. 3 with different distances. In typical nice weather, the link loss is measured to fluctuate between 66 dB and 83 dB, with an average of 74 dB, which is consistent with the calculation value.

The total link loss of the 113-km horizontal free-space channel does not reach the tolerated maximum value of our system. According to the simulation results, the total telescope link loss of 190 km distance is 89 dB, which is comparable with the average telescope link loss of the misaligned link curve in Fig.2 of the main text. So it can be predicted that the limit transmission distance of our system should be around 190 km.

Note that the r0 of the atmospheric is much smaller than the aperture of the telescope, the multipath issue exists. In our setup, spatial filtering is inserted by the single mode coupling to greatly reduce the influence of the multipath issue. For the satellite-ground link of several thousands of kilometers, the atmospheric turbulence is actually less than that of the 113 km near ground link, so that the multipath issue should not be a problem.

3 Linear optical sampling electronic system

The architecture of the LOS electronic system is illustrated in Fig. 4, consisting of a GPS receiver, a Gigabit Ethernet switch and two LOS electronic modules, one for the 1545 nm comb link and the other for the 1563 nm comb link. Inside the LOS electronic module, the optical interference signals between the received comb and local comb are fed into a balanced detector. After passing through a low-pass filter with 100 MHz bandwidth, the interferogram voltages are digitized by a 14-bit ADC, and then the digitized data streams are transmitted to a FPGA, which is responsible for digital processing. Both the clocks of ADC and FPGA are synchronized with the repetition frequency of the local comb, which is implemented by a photodetector (PD) and phase-locked loop (PLL) circuits integrated in the hardware.

The GPS receiver is used to synchronize the start time between different terminals, by generating a pulse per second (PPS) signal to the LOS electronic module with 30 nanosecond time precision. Once the FPGA controller detects the first PPS signal after receving the data acquisition start command, a 64-bit binary counter starts counting for timestamp recording. When the amplitude of the interferogram signal is above a given threshold, the current timestamp of the trigger point is recorded. The relative position of the interferogram peak value is obtained through a peak searching function implemented in the FPGA, and data with a window of 1024 sampling points around the peak is extracted and transferred to the computer via Gigabit Ethernet for data storage and further analysis.

As mentioned above, one data frame includes 1024 sampling points, and each point is a 16-bit binary data. The raw data rate of 5 M byte per second will be generated assuming that the repetition frequency difference of the two combs is 2.5 kHz. In this case, it will take a lot of time to process the whole data after hours of data storage, therefore real-time data processing becomes necessary. Once an hour of data is stored, the phase calculation program will run. Then the processed results of the each site will be transferred to the central server computer for further processing, which combines the time data from both terminals and calculates the clock time offset and transfer instability.

The detailed post-processing procedure is given as follows. First, we have four groups of data, named "1545 A/B" and "1563 A/B". Each group of data includes one-way time measurement results and corresponding timestamps. Second, we calculate the clock offset for 1545 link by combining 1545 A/B data. In the combining process, we set a gate time and make pairs between the two group of data so that the difference of timestamps in each pair is smaller than the gate time. The data, which couldn't be paired, will be deleted in this step. Based on the paired data, the clock offset and link delay of 1545 link are calculated. The gate time in our program is $1/(2\Delta fr_{1545})$, where Δfr_{1545} is the difference of repetition rate of the two 1545 combs. The same program is used to process 1563 link, with the gate time changed to $1/(2\Delta fr_{1563})$. Finally, we use the same program to process clock offsets of 1545 link and 1563 link. By finding the corresponding pairs between the two link offsets data, the difference of clock offsets is calculated. Because we filter some data in the post-processing step, the timestamps of the difference of clock offsets are not uniformly distributed. Here, we suppose that the time interval is similar, so that we use the average valid sampling time as the gate time to calculate the MDEV.

4 Optical transceiver telescope

The 1545 nm OFC and 1563 nm OFC were used for optical two-way time and frequency transfer over free space separately, which requires the establishment of two atmospheric links. A schematic layout of the transceivers is shown in Fig. 5, which includes the main telescope, the optical components, and the electronics. This scheme can verify the impact of the asymmetric path between the transmitter and receiver on the performance of time-frequency transfer due to the point ahead angle issue in satellite-ground case. We use three polarizing beam splitters (PBS) to design asymmetric transmit and receive paths, with single horizontal (H) or vertical (V) polarization for each direction beam. In transceiver of one terminal, the H-polarized beam passes through the transmit path, the V-polarized beam passes through the receive path, and vice versa in the other terminal. Polarization-maintaining fibers are exploited to collect light and to ensure high H(V) polarization contrast ratio. The reflector (MIR) in the transmit path simulates a ground-based fast steering mirror for compensation to the point ahead angle.

The delay difference between the transmitting and receiving paths is affected by temperature fluctuations, and we use optical bench to build asymmetric transmitter and receiver to solve this problem. The materials of optical devices such as PBS, MIR and dichroic beam splitter (DM) are fused silica with low thermal expansion coefficient ($5 \times 10^{-7}/^{\circ}C$). The yellow rectangles in the Fig. 5 represent large fused silica platforms with size of 170*150*30 mm and 190*140*30 mm for both terminal, respectively. In addition, the asymmetric path between transmit and receive is less than 150 mm. The deformable mirror (DMIR), which integrates electronics and optics, is not on the fused silica optical bench, because devices of such high complexity are difficult to be integrated with optical bench. We add temperature control in the blue rectangular part (Fig. 5) to reduce the optical paths variations of both the DMIR and the optical bench.

There are two functions employed to resist atmospheric turbulence and improve the single mode fiber coupling efficiency. One function is the fast-steering-mirror (FSM)-based fine tracking system, which is used for correcting lower-order aberrations. The central wavelengths of the beacon lights are 785 nm and 915 nm, respectively. The power of 785 nm and 914 nm laser is 200 mW and 400 mW, respectively. In the receiver, the fine tracking complementary metal–oxide semiconductor (CMOS) camera detects the tilt-type aberrations via the incoming beacon laser. It then guides the FSM driven by piezoceramics to perform the correction with a closed-loop bandwidth of 100 Hz. The other function is the adaptive optics (AO) system, which is based on a deformable-mirror (DMIR) here. The AO system can correct higher-order aberrations of the wavefront introduced by the atmosphere. The beacon laser is shared in the receiver and divided into two parts, $\sim$30% for the fine tracking and $\sim$70% for the AO system. A modal version of the stochastic parallel gradient descent algorithm (M-SPGD) is employed for AO. The coupled power of SMF is the performance metric in the M-SPGD algorithm, which can be found in more detail in our previous work[6]. We utilize a silver-coated DMIR with 97 actuators. In addition, an avalanche photo-detector (APD) is used to detect the coupled power of the reference beacon laser. The AO reference laser before entering the APD is about 2 nW.

The DRI in Fig. 5 is controller of DMIR. The wavelength division multiplexing (WDM) separates the beacon light from the 1545 nm signal. The DM6 and DM7 reflect 70%-75% of the beacon light into the receiver, and pass 25%-30% to the CMOS. The fine tracking system includes the FSM, DM6(DM7), MIR and CMOS. Another CMOS camera and telescope controller are employed to build a coarse tracking system, which is used to mainly compensate the long term drift of the mechanical structure of the telescope. The primary mirror of the transceiver terminal is a reflecting Cassegrain telescope with an aperture of 400 mm and ×16 magnification. The telescope magnification is totally ×48 with a ×3 magnification beam expander (BE) added in the transceiver. In addition, we also design 1605FC to transmit and receive optical signals with the central wavelength of 1605 nm for laser communication, which is employed in the real-time synchronization operation.

5 High-power low phase noise optical frequency comb

The high precision time-frequency link measurements presented here contain four high-power frequency combs based on Er-fiber mode-locked lasers. These frequency combs are almost identical except for the repetition rates and central wavelengths. A schematic of one frequency comb is shown in Fig. 6. The key elements of frequency combs are fiber oscillator, carrier-envelope offset frequency detection, and the pulse amplifier. The oscillator is mode locked with an all polarization-maintaining nonlinear amplifying loop mirror. The PZT and EOM are inserted into the laser cavity for repetition rate control. The average output power of the oscillator is $\sim$1 mW and the pulses allowed for sub-100 fs pulse duration if compressed in standard fiber.

A part of the pulse train of the oscillator ($\sim$0.5 mW) is used for determining the carrier-envelope offset frequency of the Er-fiber oscillator. The oscillator is followed by an EDFA, a 15-cm HNLF for octave-spanning supercontinuum generating, and a PPLN to double the supercontinuum light at 2000 nm. The common-path f-2f interferometer is adopted for carrier-envelope offset frequency measurement. The signal-to-noise ratio of carrier-envelope offset frequency signal is more than 35 dB in a 300 kHz resolution bandwidth (RBW).

The pulse amplifier consists of the pulse stretcher, the preamplifier, and the power amplifier. The pulse stretcher adopts Chirped fiber Bragg grating with a reflectivity of 50% and a bandwidth of 60 nm centered at 1560 nm, resulting in a pulse duration of 120 ps. And then the light is launched into a 20-nm bandpass filter. To compensate for the loss of Chirped fiber Bragg grating and the 20-nm bandpass filter, the pulse train is amplified in a preamplifier, which is forward and backward pumped with a 800-mW 976-nm laser diodes. The pulses are amplified up to 120 mW. The power amplifier is comprised of a 200-cm-long polarization-maintaining double-clad Er-Yb co-doped fiber with a 10-μm core diameter and 130-μm cladding diameter that is forward-pumped by a high-power fiber-coupled multimode diode at 976 nm through a signal-pump combiner. The cladding power stripper (CPS) is placed after the power amplifier to strip the residual pump. The fiber of the output port of CPS and the second 20-nm bandpass filter are PM1550, which is single-mode at 1550 nm.

After amplification, we achieve more than 1 Watt of average output power. The amplified pulses has a 11-14 nm bandwidth (-10 dB) centered at 1545 nm or 1563 nm and durations of 60-100 ps assuming a gaussian-form profile. Figure 7 shows the measured spectra of the pulses from BPF. The measured autocorrelation traces and the corresponding Gaussian fitting curves of the power amplifier are shown in Fig. 8. To evaluate the characterization of comb stabilization, the carrier-envelope offset frequency and the beat frequency are measured by directly countering at 1 second gate time. The fractional frequency stability is plotted in Fig. 9.

The short-term instability is relatively high , which is mainly caused by the use of high-power amplified combs. The hort-term stability is mainly limited by the time jitter of single interference and valid interference rate. Here, the timing jitter is around 40-60 fs, which is relatively high, mainly caused by the fact that dual combs dispersion consistency is poor, corresponding to a large interference time. Compared to low-power comb systems, the comb interference time is increased from 3 ps to 7 ps. In principle, this effect can be minimized by carefully dispersion management.

6 The fiber link noise

The noise of the aerial optical fiber is much larger than the noise of the atmosphere. To estimate the noise intensity of the fiber link, we record the frequency of the driver signal for AOM 1 which is used to compensate for the Doppler noise in the fiber link. The relative phase drift of the link can be calculated from the frequency data. The result is shown in Fig. 10. The frequency noise of the fiber link can be up to several kilohertz and the phase drift is hundreds of nanoseconds, almost two orders of magnitude larger than the free-space link.

7 The original one-way free-space links and fiber link data

The time variations of the phase data for four one-way free-space links and the clock offset of the fiber link are shown in Fig.11, which is the 10 s averaged data of the raw data. The phase data obtained from the optical comb interferogram of the sampling system include the phase difference of two ultra-stable laser and the change of flight time. Because we use two independent ultra-stable lasers, a nearly linear drift can be observed for short terms, resulting in a quadratic curve of the clock offset ΔT. The change of flight time is several nanoseconds, which is much smaller than the accumulative time variation due to ultra-stable laser drift. Therefore, the phase curves of the one-way time-of-flight and the clock offset measured by the fiber link are indistinguishable. There are a few breaks for the fiber link, which is attributed to sudden large noise and poor signal-to-noise (SNR) of the fiber link due to 70% of the link fiber is aerial.

8 Real-time synchronization

As we mentioned, the free-space link can support real-time processing and synchronization.

The synchronization experimental setup is shown in Fig. 12. At both terminals (Nanshan and Gaoyazi) the OFCs with wavelengths of 1563nm and 1545nm are locked to USLs, which are the reference clock sources. The interference pulses between local and received comb are detected by the LOS module, and then the detected interferograms are processed by a FPGA controller. To synchronize the time at two remote terminals, three conditions should be satisfied, i.e. real-time measurement of time offset, real-time data communication and real-time clock offset adjustment. Therefore, the phase calculation algorithm is implemented in the FPGA and a laser communication link is utilized. The calculated phase information of terminal A, ΔT_A, is transferred to terminal B over the 113km free-space laser communication link after coding and electro-optical conversion. Once obtained at terminal B, the ΔT_A is combined with local calculated phase information of site B, ΔT_B, to calculate the clock offset ΔT_{AB}. Then through proportional integral (PI) loop filter and direct digital synthesizer (DDS), a feedback signal which represents clock offset is generated. An acoustic optical modulator (AOM) is driven by this feedback signal, which is applied to adjust the local reference clock offset relative to the master clock of terminal A. With a 5-Hz feedback bandwidth, the two terminals are synchronized via the 1563 comb link. Besides, the synchronization verification is also carried out via an out-of-loop measurement of the time offset in the 1545 comb link.

Figure 13 shows the results of the synchronized 113-km free-space link with an average link loss of 80 dB. The fractional frequency stability of in-loop link and out-loop link reach 2.4×10^{-20} and 1.6×10^{-19} at 10,000 s, respectively.

References

1. Milonni, P. W., Carter, J. H., Peterson, C. G. & Hughes, R. J. Effects of propagation through atmospheric turbulence on photon statistics. Journal of Optics B: Quantum and Semiclassical Optics **6**, S742–S745 (2004). URL https://doi.org/10.1088/1464-4266/6/8/018.

2. Strohbehn, J. W. (ed.) *Laser Beam Propagation in the Atmosphere*, vol. 25 of *Topics in Applied Physics* (Springer Berlin Heidelberg, Berlin, Heidelberg, 1978). URL http://link.springer.com/10.1007/3-540-08812-1.
3. Kim, I. I., McArthur, B. & Korevaar, E. J. Comparison of laser beam propagation at 785 nm and 1550 nm in fog and haze for optical wireless communications. In Korevaar, E. J. (ed.) *Optical Wireless Communications III*, 26–37 (2001). URL http://proceedings.spiedigitallibrary.org/proceeding.aspx?articleid=895905.
4. Dikmelik, Y. & Davidson, F. M. Fiber-coupling efficiency for free-space optical communication through atmospheric turbulence. *Appl. Opt.* **44**, 4946–4952 (2005). URL http://www.osapublishing.org/ao/abstract.cfm?URI=ao-44-23-4946.
5. Andrews, L. C. & Phillips, R. L. *Laser Beam Propagation through Random Media* (SPIE, 1000 20th Street, Bellingham, WA 98227-0010 USA, 2005). URL http://ebooks.spiedigitallibrary.org/book.aspx?doi=10.1117/3.626196.
6. Yang, K.-X. *et al.* Single-mode fiber coupling with a m-spgd algorithm for long-range quantum communications. *Optics Express* **28**, 36600 (2020).

Table 1: Input parameters for the total link calculation

Symbols	Parameters	Values
θ_t	divergence angle	40 μrad
V	visibility	40 km
λ	wavelength	1550 nm
C_n^2	refractive-index structure	4E-16
D_r	receiver lens diameter	400 mm
f	focal length of the receiver	1.584 m
W_m	fiber-mode field radius	5 μm

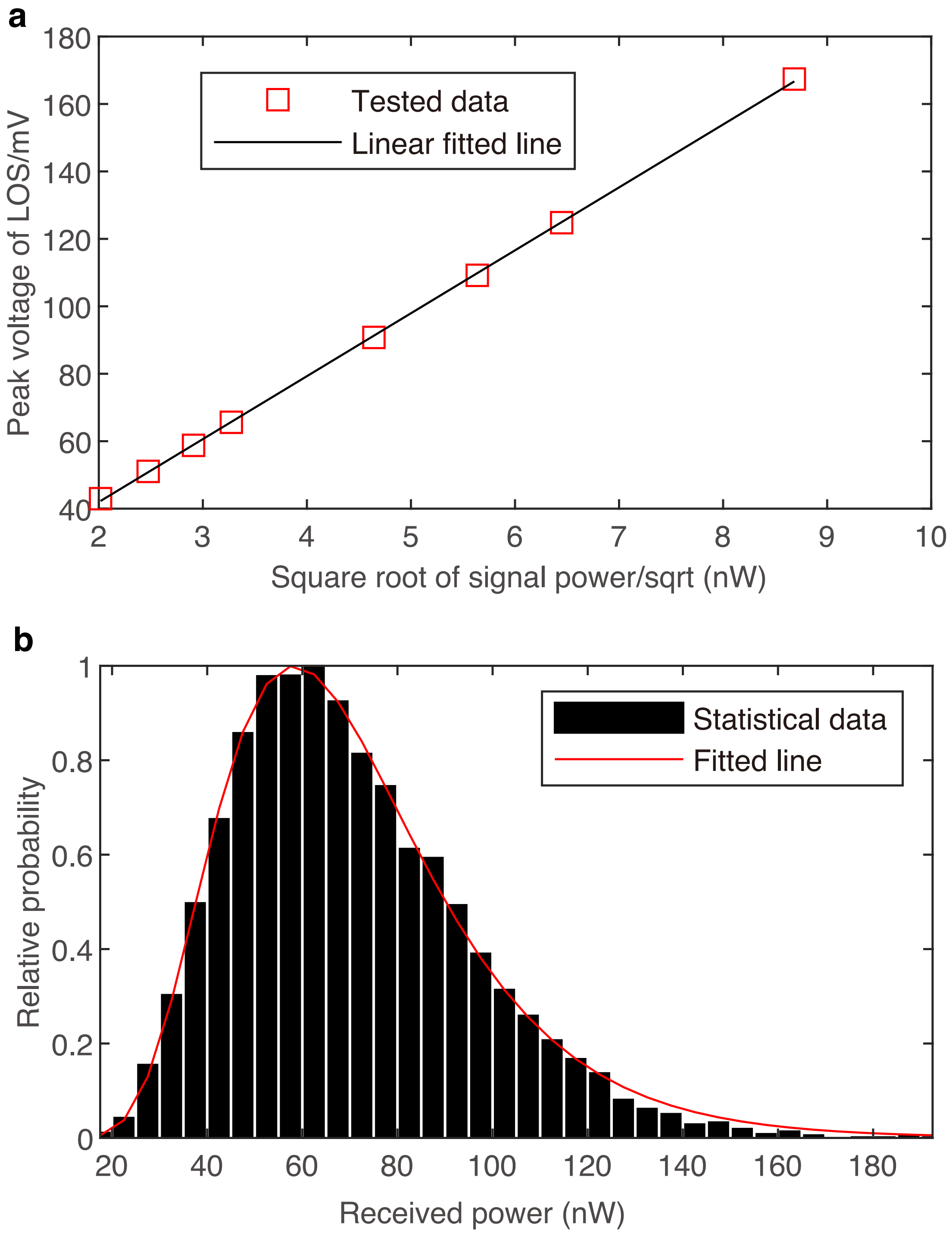

Figure 1: (a). The relationship of peak voltage of LOS and the square root of received signal power. (b). The measured signal power distribution and the fit to the data using log-normal curve.

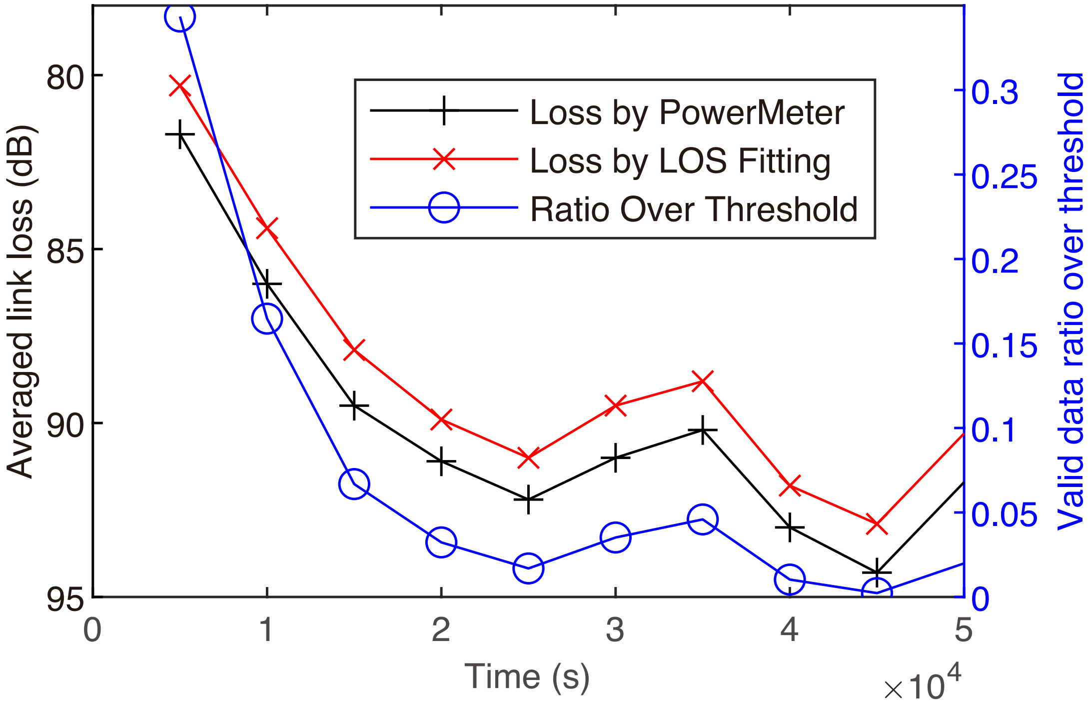

Figure 2: The average link loss calculated by the both the power meter monitoring method and the peak voltage fitting method.

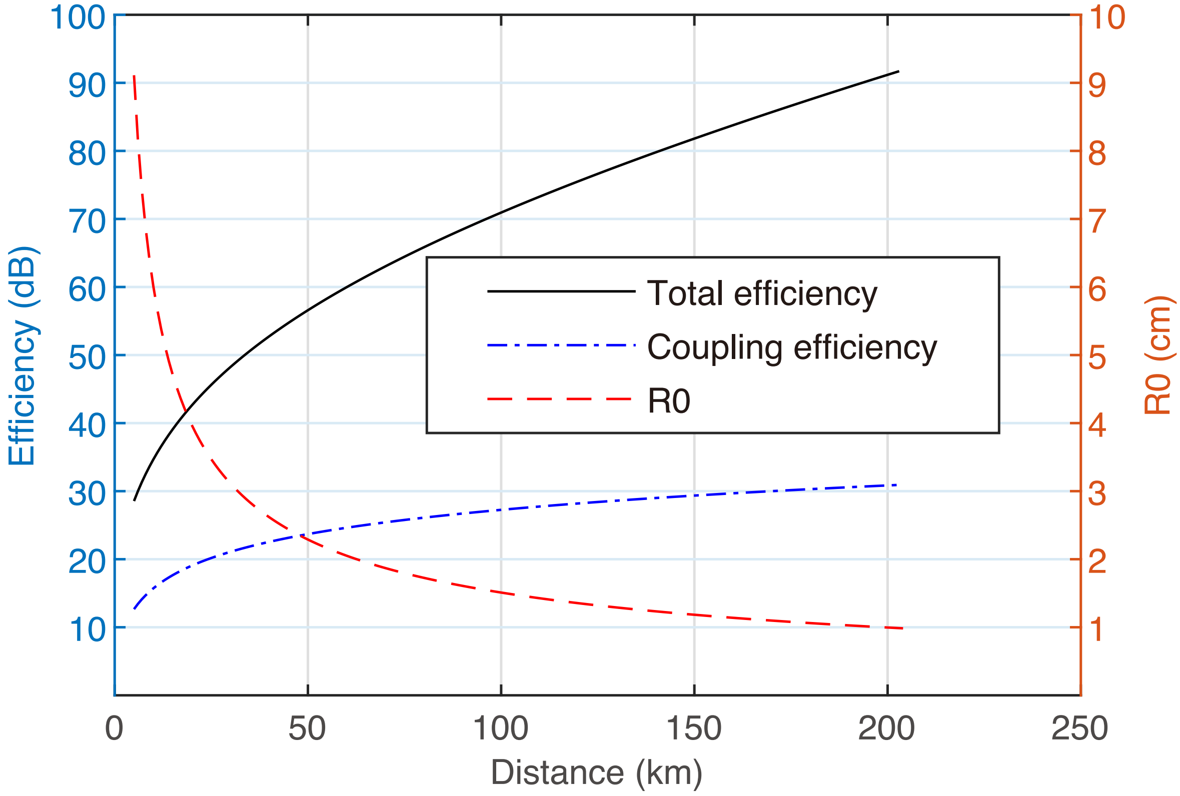

Figure 3: Extended Data Figure: Simulated r0, single-mode coupling efficiency and total attenuation change with distance.

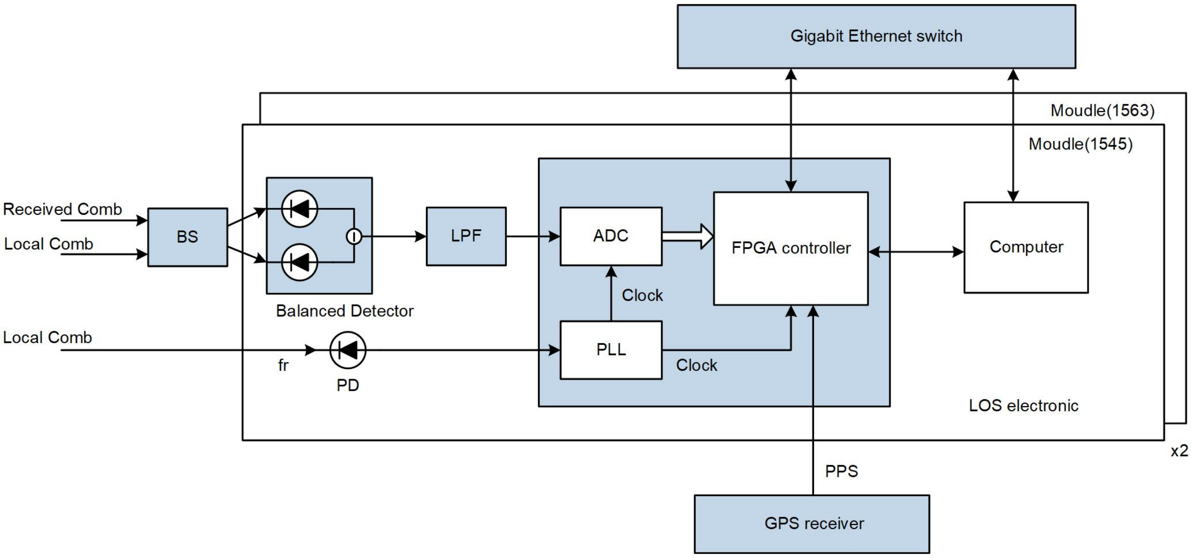

Figure 4: Architecture of the LOS electronic system.

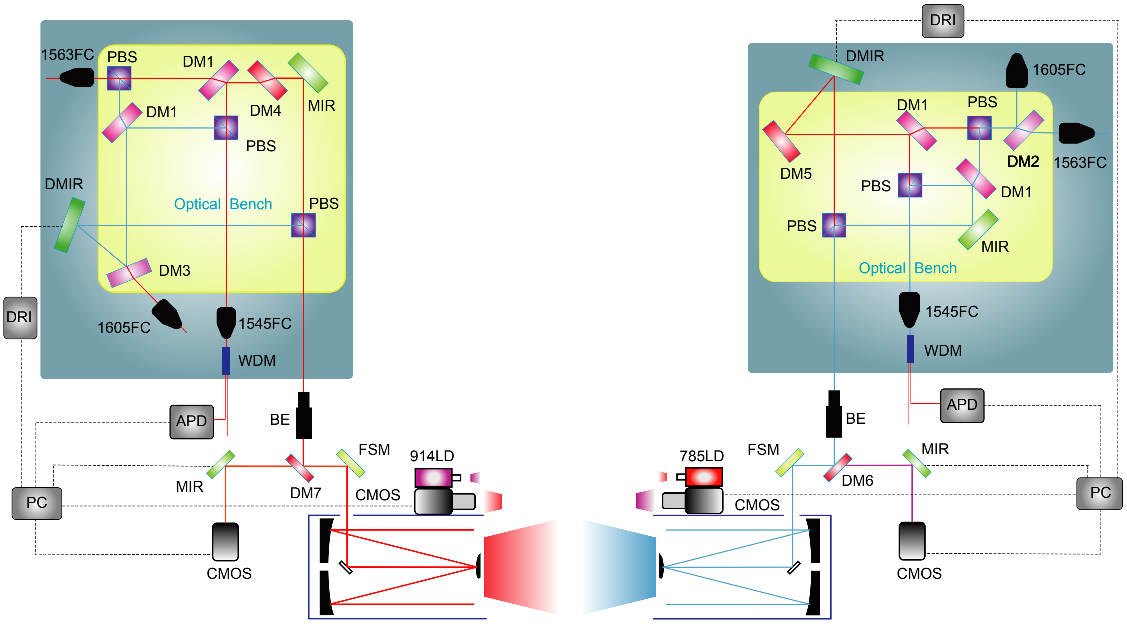

Figure 5: The optical transceiver telescope. Yellow rectangle: fused silica platforms; PBS: polarizing beam splitter; 1545FC (1563FC): fiber collimator for two-way 1545 (1563) nm comb transceiver; 1605FC: fiber collimator for laser communication transceiver; DM: dichroic beam splitter; DM1: 1563nm transmitted, 1545nm reflected; DM2: 1563nm transmitted, 1605nm reflected; DM3: 1605nm transmitted, 1545nm and 1563nm reflected; DM4: 1545nm and 1563nm transmitted, other wavelengths reflected; DM5: 1545nm and 1563 reflected, other wavelengths transmitted; DM6: ∼30% of 914 nm transmitted, other reflected; DM7: ∼30% of 785nm transmitted, other reflected; MIR: mirror; DMIR: deformable mirror; WDM: wavelength division multiplexer; BE: beam expander; APD: avalanche photo-detector; FSM: fast steering mirror; DRI: controller of DMIR; CMOS: complementary metal–oxide semiconductor; PC: processing computer.

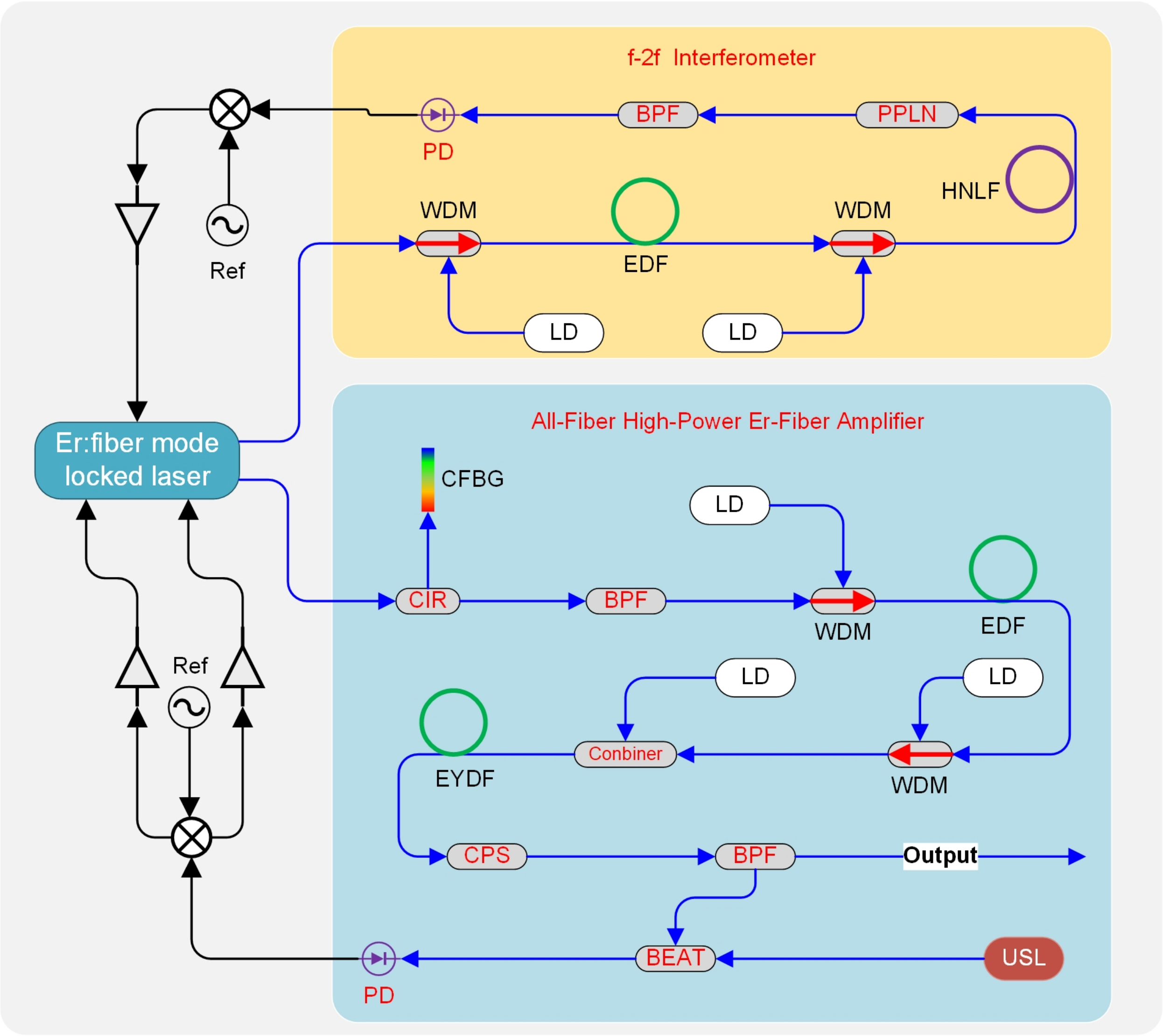

Figure 6: Schematic of high-power frequency comb. WDM, wavelength division multiplexer; ISO, isolator; EDF, Er-doped fiber; LD, laser diode; HNLF, PM-highly nonlinear fiber; PPLN, periodically-poled lithium niobite crystal; BPF, band pass filter; PD, photo detector; CIR, circulator; CFBG, Chirped fiber Bragg grating; Combiner, pump and signal combiner; CPS, cladding power stripper; USL, ultra-stable laser.

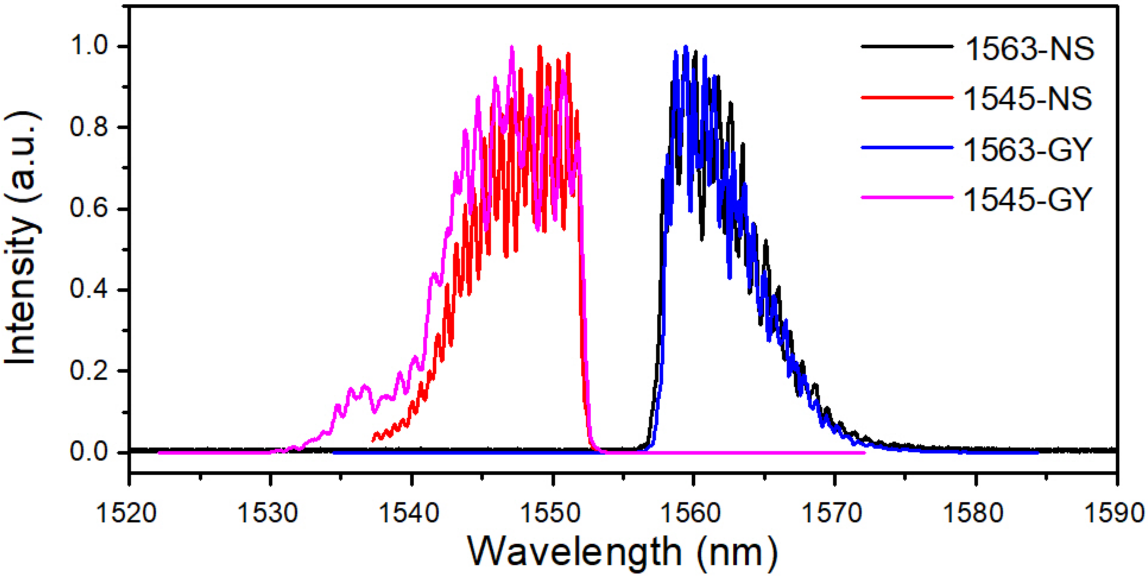

Figure 7: Measured spectrum of high-power amplifiers.

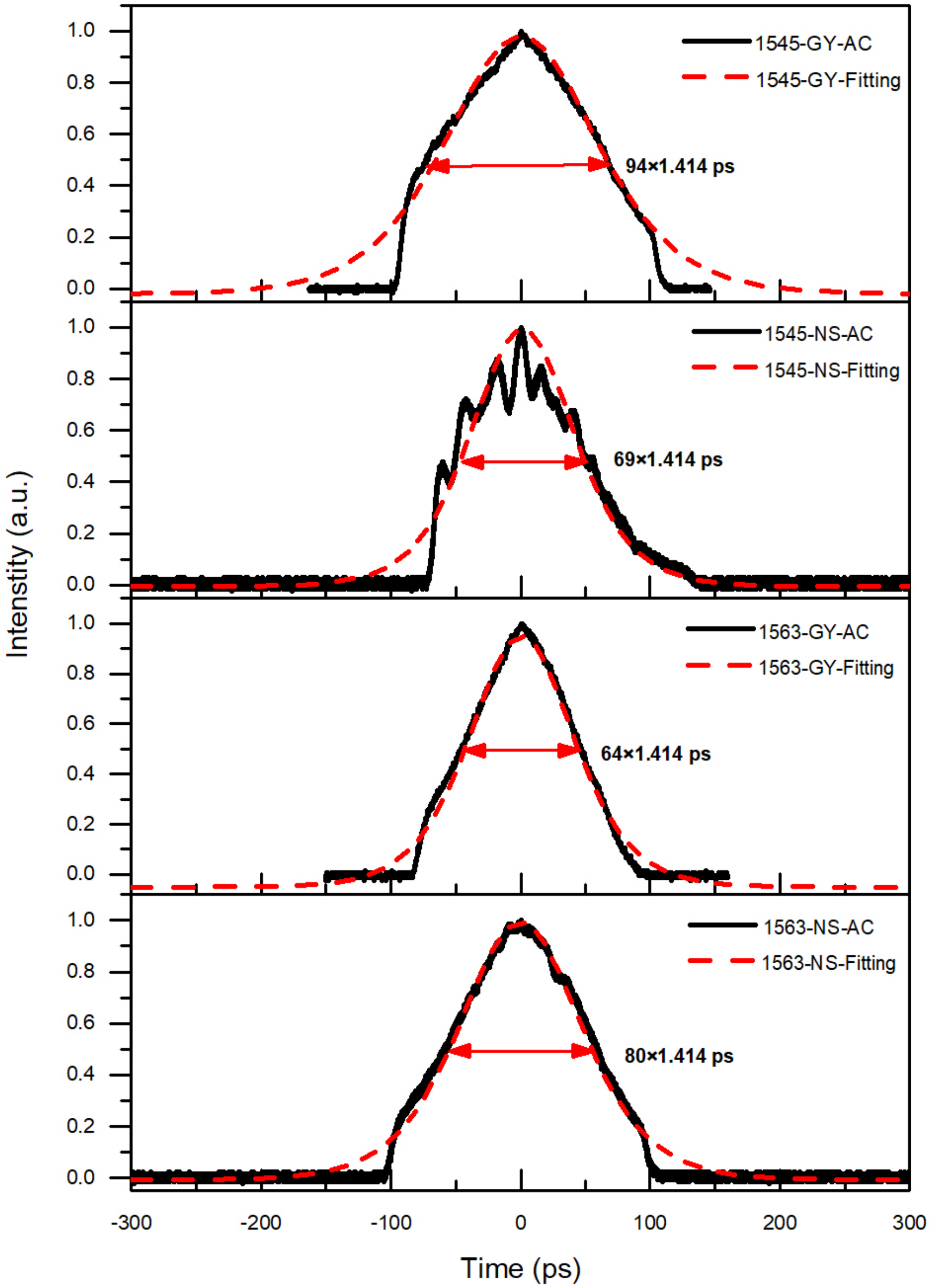

Figure 8: Autocorrelation trace of high-power amplifiers.

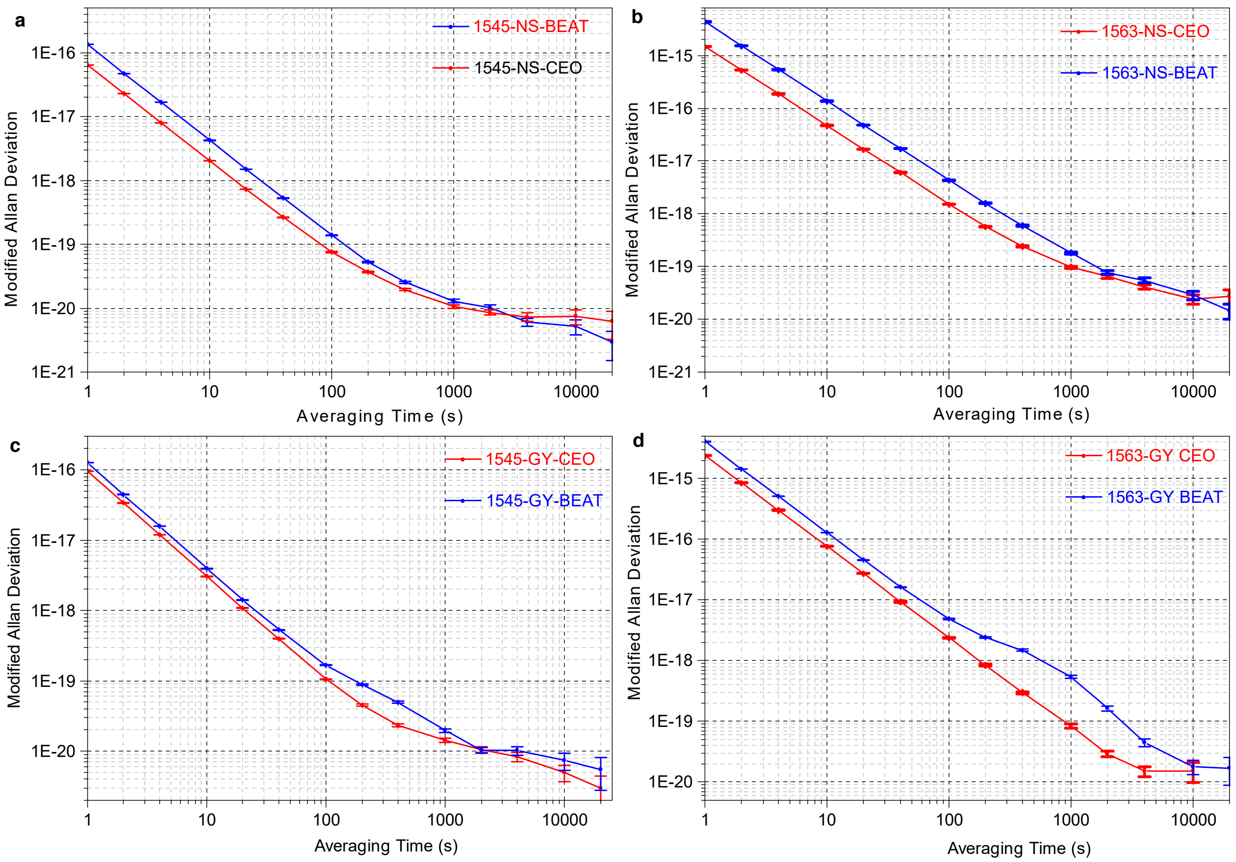

Figure 9: Fractional frequency stabilities of combs.

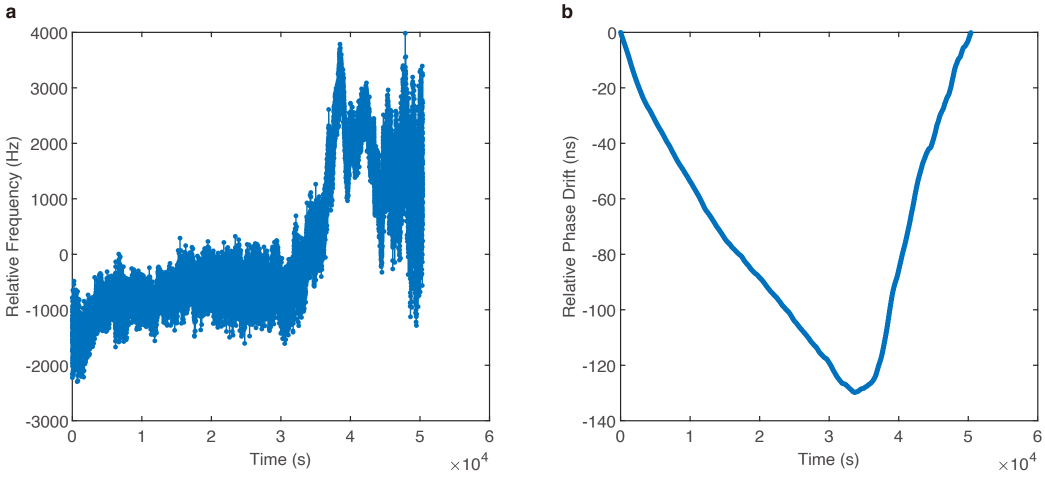

Figure 10: (a) The frequency of driver signal for AOM 1 relative to its center value. The AOM 1 is used to compensate for the Doppler noise in the fiber link. So the changing of the frequency implies the changing of doppler noise. (b) The accumulated phase change in the link. This is integral for the frequency data at the subfigure (a).

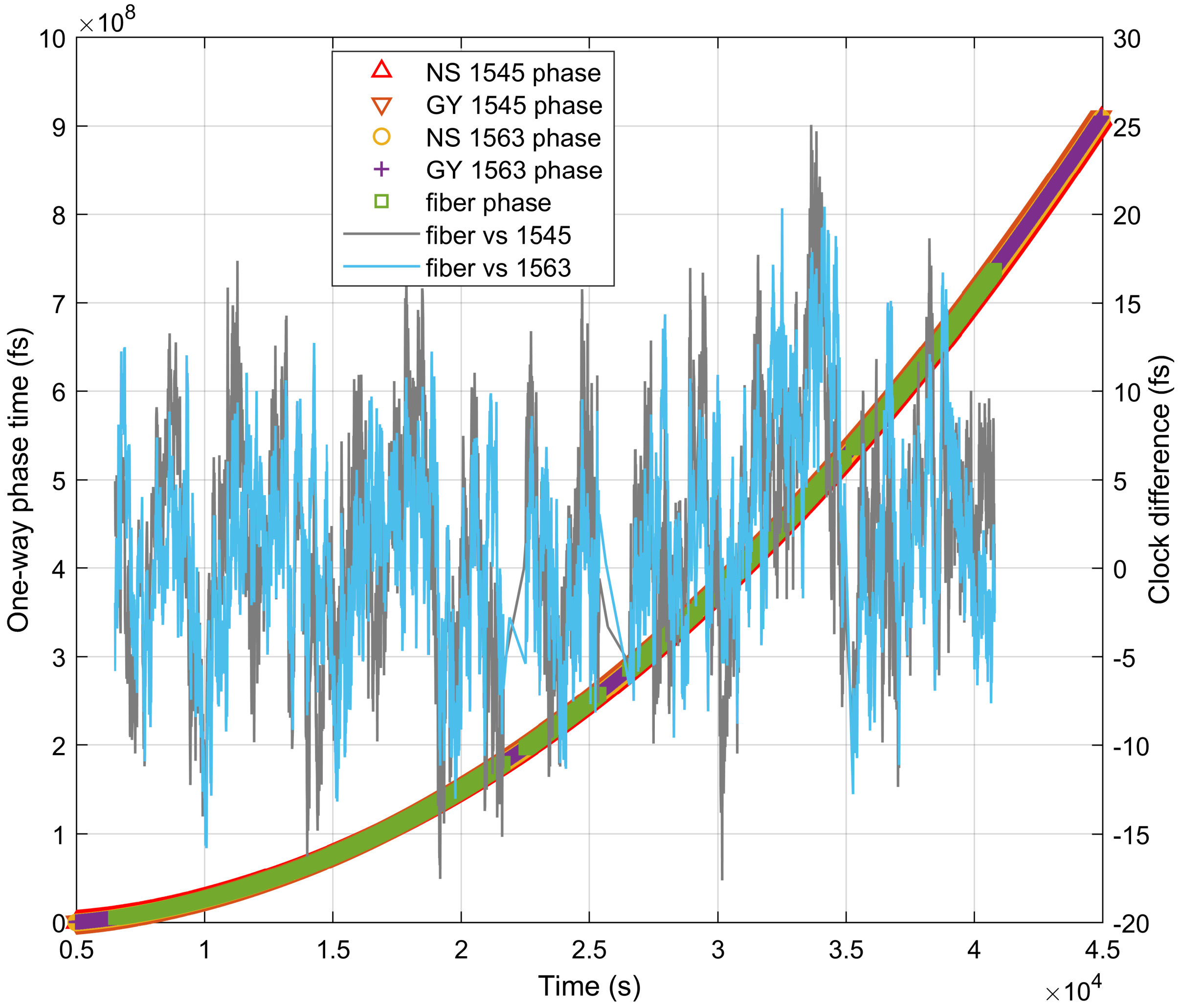

Figure 11: The time variations of one-way free-space links, where the time variation measured by the1545 nm optical combs in NanShan (NS) station is in red (up triangle), 1545 nm optical comb in Gaoyazi (GY) station (orange down triangle), 1563 nm optical comb in NS station (yellow circle) and 1563 nm optical comb in GY station (purple cross), the clock offset measured with the fiber link (green square, left axis). Difference of clock offset (marked with right axis) between 1545 nm optical comb and fiber link (gray line), 1563 nm optical comb and fiber link (light blue line) are shown in the figure as well.

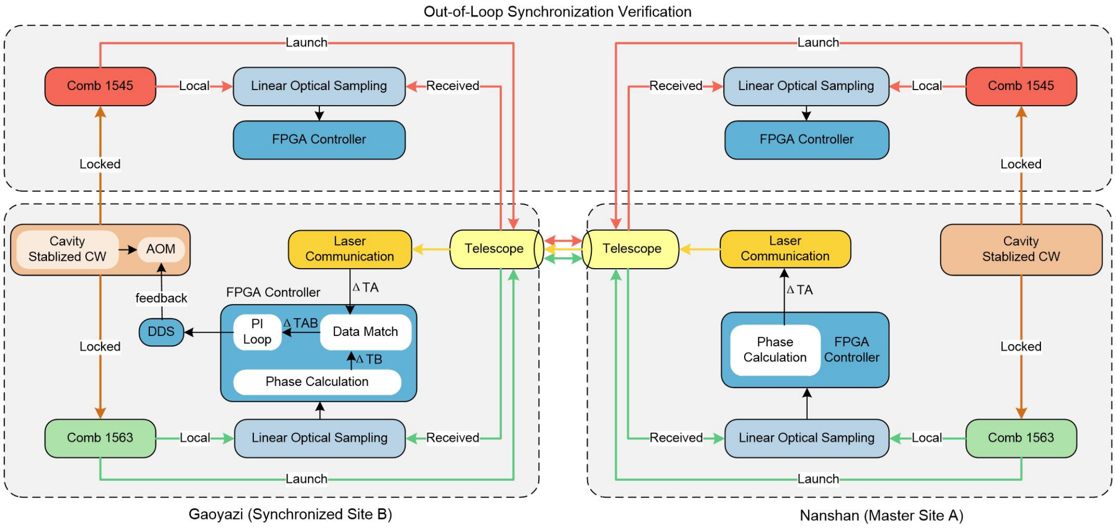

Figure 12: Synchronization experimental setup.

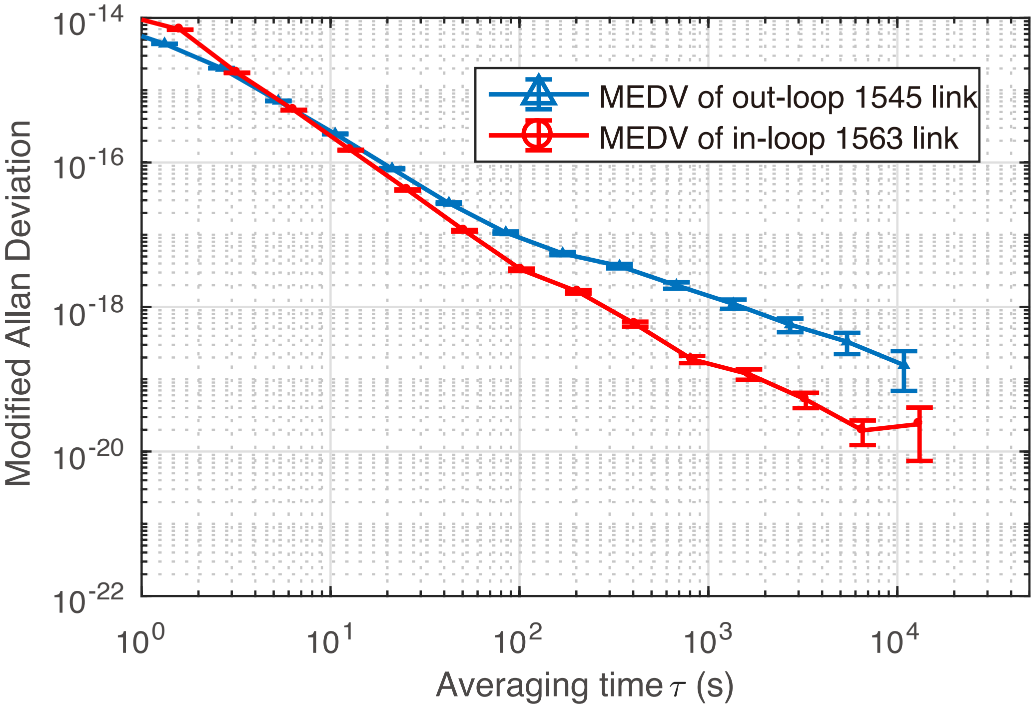

Figure 13: Modified Allan Deviation for the synchronized time-frequency link.